

## IN-SITU SERIES CONNECTION FOR THIN FILM PHOTOVOLTAIC MODULES

R. Merz<sup>1,3</sup>, M. M. Adachi<sup>2</sup>, M. B. Schubert<sup>1</sup>, J. H. Werner<sup>1</sup>

<sup>1</sup>Institut für Physikalische Elektronik, Universität Stuttgart, Pfaffenwaldring 47, 70569 Stuttgart

<sup>2</sup>Dept. of Electrical and Computer Engineering, University of Waterloo, Canada, N2L 3G1

<sup>3</sup>corresponding author (phone: +49.711.6856.7184, fax: +49.711.6856.7143, email: rainer.merz@ipe.uni-stuttgart.de)

**ABSTRACT:** The in-situ series connection of 10 amorphous silicon based solar cells on a flexible polymer foil yields a photovoltaic module with an efficiency  $\eta = 3\%$ . Masking wires pattern all constituting layers of the thin film solar cells during their subsequent deposition steps. Appropriate wire shifts provide electrical isolation and monolithic series connection of the single solar cells into a photovoltaic module with an open circuit voltage  $V_{oc} = 9$  V. The wire set initially patterns the back contact, a first wire shift masks the back contact during the cell deposition and a second one opens the back contact to provide series connection during deposition of the transparent front contact. The present work discusses three different configurations of the in-situ series connection resulting in interconnection losses  $F < 15\%$ .  
**Keywords:** Amorphous Silicon, Flexible Substrate, Module Manufacturing

### 1 INTRODUCTION

Thin film solar cell fabrication enables integrated series connection [1]. On glass substrates, laser patterning isolates single cells and creates an integrated series connection to form photovoltaic modules. On flexible substrates such as plastic foil the integrated series connection is more difficult to control and to optimize.

This paper evaluates three possibilities for our novel in-situ series connection (ISS) [2]. The ISS allows for monolithic series connection of thin film solar cells on flexible foils like polyethylene-naphthalate (PEN). Thin wires mask the substrate for patterning the layers during deposition. To provide monolithic series connection, the position of the wires shifts twice between depositions. Several possibilities for repositioning of the wires and the corresponding calculation of losses are presented. An experimental ISS module yields an efficiency of  $\eta_{ISS} = 3\%$

### 2 IN-SITU SERIES CONNECTION

Here, the ISS uses amorphous silicon (a-Si) solar cells in n-i-p configuration. Masking the substrate with wires of diameter  $d_w = 200$   $\mu\text{m}$  during the deposition of the layers allows for series connection of adjacent cells.

Figure 1 illustrates the monolithic series connection of an ISS module. The preparation of n-i-p cells starts with the deposition of silver as back contact. The masking wire set separates the back contact into stripes

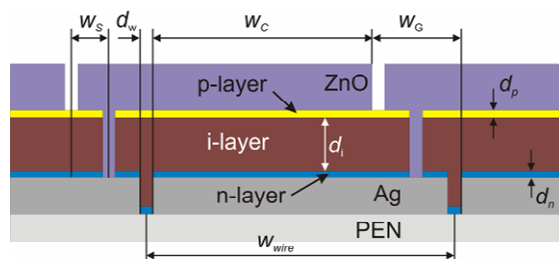


Figure 1: Cross section of monolithic series connection by wire masking. Wires of distance  $w_{wire}$  mask substrate during deposition. Two wire shifts between subsequent layer depositions provide series connection gap  $w_c$ , depending on wire diameter  $d_w$  and shift  $w_s$ .

with the distance  $d_w$ , the wire diameter. A shift  $w_s = 0.5$  mm of the wire masks the back contact during the deposition of the amorphous and microcrystalline silicon ( $\mu\text{cSi}$ ) layers. A phosphorous doped n-type (n) layer of thickness  $d_n$ , an intrinsic (i) film of thickness  $d_i$ , and a boron doped p-type (p) layer of thickness  $d_p$  form the solar cell.

A second wire shift isolates the front contacts of the cells and creates a series connection between back and front contacts of neighboring cells. This study examines three different configurations of the integrated series connection.

#### 2.1 Wire shifts

Figure 2 depicts the possibility ISS-A of the layer configuration for the ISS. The wire set initially masks the PEN substrate during the evaporation of the silver back contact. After deposition of the back contact, a wire shift repositions the masking wires to the left. Deposition of the n-type layer of resistivity  $\rho_n = 0.02$   $\Omega\text{cm}$  results in a shunt resistance  $R_{p,BC}$  between the back contacts of neighboring cells. The resistance  $R_{p,BC} = \rho_n d_w / d_n L$  decreases with decreasing wire diameter  $d_w$  and with increasing length  $L$  of the module which is not shown in the 2-dimensional sketch of Fig. 2. The subsequent deposition of the i- and p-layers completes the thin film diode. The last wire shift exposes the back contacts of the cells, and deposition of Al-doped zinc oxide (ZnO) connects the front contact of one cell to the back contact of the adjacent one. To prevent short circuits, the wires also separate the front contacts of the cells. The p-type layer of thickness  $d_p$  and resistivity  $\rho_p = 0.3$   $\Omega\text{cm}$  forms a

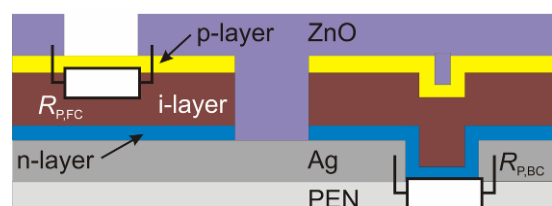


Figure 2: Configuration ISS-A with wire shifts after back and front contact depositions. This configuration introduces two resistances  $R_{p,BC}$  and  $R_{p,FC}$  in parallel to the single cells.

shunt resistance  $R_{p,FC} = \rho_p d_w / d_p L$  between the front contacts of adjacent cells.

Figure 3 presents the configuration ISS-B with wire shifts after the depositions of the back contact and the intrinsic layer. A similar first wire shift as in ISS-A yields the shunt resistance  $R_{p,BC} = \rho_n d_w / d_n L$ . The second wire shift after i-layer deposition prevents the parasitic front side resistance  $R_{p,FC}$  between adjacent cells.

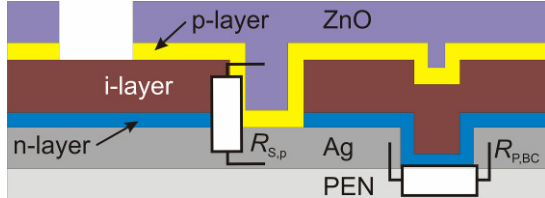


Figure 3: Configuration ISS-B with wire shifts after Ag and i-layer depositions yields a series resistance  $R_{S,p}$  at the p-layer/back contact interface, but avoids  $R_{p,FC}$ .

The wire shift after i-layer deposition prevents the parasitic resistance between adjacent front contacts, but the p-layer covering the back contact leads to a series resistance  $R_{S,p} = \rho_p d_p / d_w L$ .

Figure 4 illustrates configuration ISS-C with wire shifts before and after i-layer deposition. The resistance  $R_{S,pn} = \rho_p d_p / d_w L + \rho_n d_n / d_w L$  represents the ohmic losses of the doped layers which form a parasitic p-n layer stack between the ZnO front contact and the back contact within the gap between adjacent cell stripes.

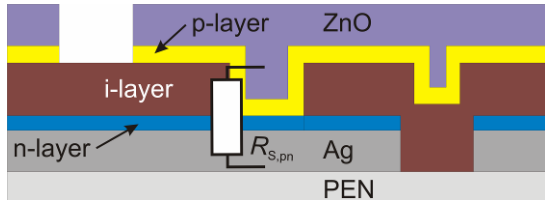


Figure 4: Cross section of ISS-C prepared by wire shifts before and after i-layer deposition.  $R_{S,pn}$  represents the ohmic losses due to the p-n layer stack in the cell gaps.

## 2.2 Discussion

To maximize the module efficiency, our module optimization recalculates a measured current density  $J$  vs. voltage  $V$  characteristics of single cells with the parasitic ohmic losses of the different ISS configurations A, B and C. The cells deposited on PEN consist of a microcrystalline n-layer (n- $\mu$ cSi) of thickness  $d_n = 50$  nm and resistivity  $\rho_n = 0.03$   $\Omega$ cm, an i-layer of thickness  $d_i = 400$  nm and a microcrystalline p-layer (p- $\mu$ cSi) of  $d_p = 45$  nm and resistivity  $\rho_p = 0.3$   $\Omega$ cm.

Figure 5 compares the  $J/V$ -characteristics of a reference cell with a fill factor  $FF_{ref} = 47.0$  % with recalculated curves taking parasitic resistances of the configurations ISS-A, -B and -C into consideration. The parasitic losses  $R_{p,BC}$  and  $R_{p,FC}$  of ISS-A decrease the current density to  $J_A = J_{ref} + V_{ref} / Lw_C (R_{p,BC} + R_{p,FC})$  and the fill factor to  $FF_A = 27.1$  %.

The parasitic series resistance  $R_{S,FC}$  of ISS-B reduces the output voltage of a single cell to  $V_B = V_{cell} - (J_{cell} R_{S,FC} / Lw_C)$ , the current density to  $J_B = J_{ref} + V_B / R_{p,BC}$  and the fill factor to  $FF_B = 27.9$  %. In ISS-C, the output

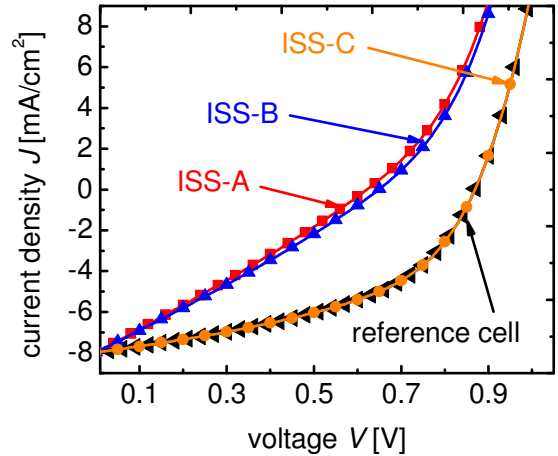


Figure 5: Recalculated  $J/V$ -characteristics of ISS configurations with different wire shifts. ISS-A exhibits parasitic shunt resistances  $R_{p,BC}$  and  $R_{p,FC}$ , ISS-B shunt and series losses  $R_{p,BC}$  and  $R_{S,FC}$ , and ISS-C only minor series losses  $R_{S,pn}$  at the interconnection interfaces.

voltage  $V_C = V_{ref} - (J_{ref} R_{S,pn}) / (Lw_C)$  only slightly decreases, but yielding the best fill factor  $FF_C = 47.0$  %.

Recalculating the configurations with a typical higher resistivity  $\rho_{n-aSi} = 100$   $\Omega$ cm of n-type aSi enhances the  $FF_{A,n-aSi} = 43.8$  % and  $FF_{B,n-aSi} = 47.0$  %, but does not effect  $FF_{C,n-aSi} = 47.0$  %.

## 3 EXPERIMENTAL RESULTS

### 3.1 Single cells

Comparing the performance of single test cells, deposited on PEN with the same substrate clamping tool and deposition conditions as for the ISS modules, but with no wire shifts, with the  $J/V$  characteristics of an ISS-C module, validates the considerations of Sect. 2 and the results of Fig. 5.

Figure 6 depicts the clamping tool for the ISS. Some springs and a wire guide force the wire onto the substrate. The bending of the substrate guarantees an accurate contact between the wire and the surface of the substrate material.

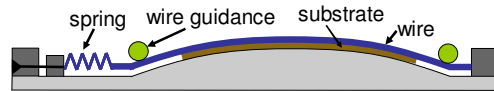


Figure 6: Springs and wire guides of the clamping tool force the wires onto the bended substrates. Accurate wire contact masks surface for layer patterning.

Figure 7 shows the  $J/V$  characteristics of nine test cells distributed over the whole area of the clamping tool. The cell with the best fill factor  $FF_{MAX} = 50.5$  % yields an efficiency  $\eta_{MAX} = 3.6$  %, the one with the worst  $FF_{MIN} = 38$  % an efficiency  $\eta_{MIN} = 2.6$  %. The average open circuit voltage  $V_{OC,av} = 870$  mV, short circuit current density  $J_{SC,av} = 8.0$  mA/cm<sup>2</sup> and fill factor  $FF_{av} = 47.0$  % result in an average efficiency  $\eta_{av} = 3.3$  %.

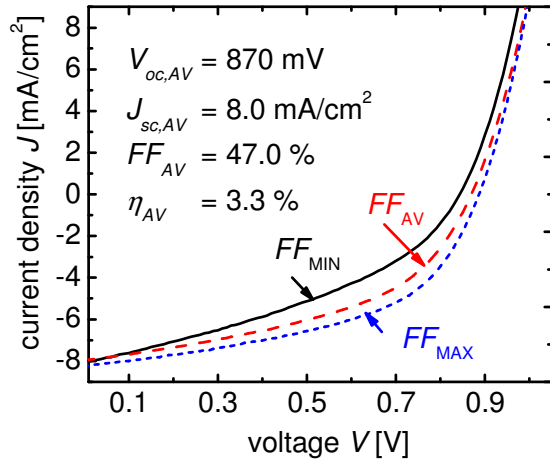


Figure 7: Cell performance on PEN deposited with the clamping tool of the ISS. An average open circuit voltage  $V_{OC,av} = 860$  mV, current density  $J_{SC,av} = 8.0$  mA/cm<sup>2</sup> and average fill factor  $FF_{av} = 47.0$  % results  $\eta_{av} = 3.3$  %.

### 3.2 Module Performance

In addition to the resistive power losses  $P_{pn} = (J_{MPP})^2 R_{S,pn} L$  of ISS-C, there are power losses  $P_G = V_{MPP} J_{MPP} w_G L$  caused by the interconnection gap, and resistive ZnO losses  $P_{TCO} = \rho_{ZnO} d_{ZnO} (J_{MPP})^2 (w_C^3 L / 3)$  with a ZnO thickness  $d_{ZnO} = 400$  nm and a ZnO resistivity  $\rho_{ZnO} = 6.8 \times 10^{-6}$   $\Omega$  [3]. Calculating the resistive losses  $P_G$ ,  $P_{TCO}$  and  $P_{pn}$  for the cells operating at their maximum power point voltage  $V_{MPP} = 630$  mV and current density  $J_{MPP} = 5.17$  mA/cm<sup>2</sup> results an optimum wire distance  $w_{wire} = w_C + w_G \approx 1$  cm for the interconnection gap  $w_G = 2w_S + d_w = 1.2$  mm.

Figure 8 represents the fractional losses  $F = (P_G + P_{TCO} + P_{pn}) / P_{max}$  of the ISS depending on the wire shift  $w_s$  for three different wire diameters  $d_w$ . The theoretical maximum power  $P_{max} = J_{MPP} V_{MPP} w_{wire} L$  of the cells discounts any losses. The used wire diameter  $d_w = 200$   $\mu$ m and wire shift  $w_s = 0.5$  mm leads to power losses  $F = 15$ %. Decreasing the wire shift  $w_s$  and diameter  $d_w$  will enhance the performance of the module. The average values of the actual cell performance and the fractional power losses  $F$  predict an open circuit voltage

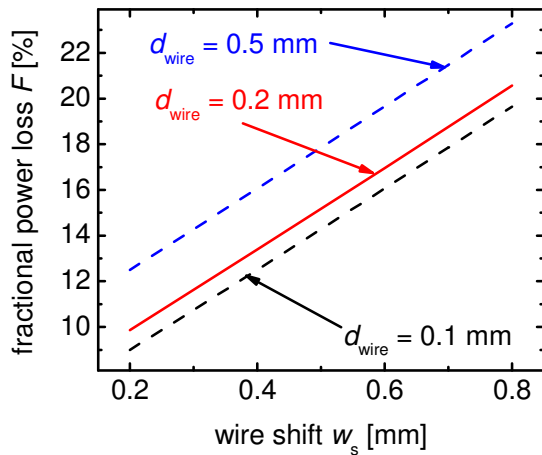


Figure 8: Fractional losses  $F$  for different wire diameters  $d_{wire}$  for ISS. Decreasing wire shifts  $w_s$  reduce the losses of the module at fixed wire distance  $w_d$ . Used  $w_s = 0.5$  mm with a wire diameter  $w_d = 200$   $\mu$ m results  $F = 15$  %.

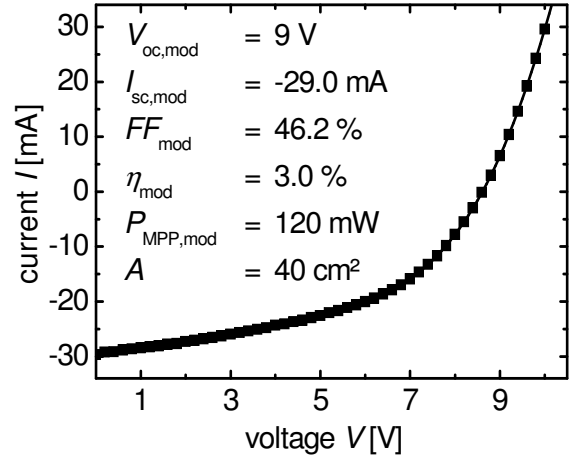


Figure 9: Module consisting of 10 cells in series with a total area  $A = 40$  cm<sup>2</sup> and an output power  $P_{MPP,mod} = 120$  mW. Measured  $V_{OC,mod} = 9$  V,  $I_{SC,mod} = -29$  mA and  $FF_{mod} = 46.2$  % verify low losses of the ISS-C configuration.

$V_{OC,predict} = 8.72$  V and a short circuit current  $I_{SC,predict} = (A/n \cdot w_G) J_{SC} = 28.08$  mA for a module of  $n = 10$  cells and an area  $A = n w_{wire} L = 40$  cm<sup>2</sup>.

For comparison, Fig. 9 presents the  $I/V$ -characteristics of an experimental ISS-C module. The measured short circuit current  $I_{SC,mod} = 29.0$  mA is even higher than the predicted one. The measured open circuit voltage  $V_{OC,mod} = 9$  V is also substantially higher than the predicted one, and the fill factor  $FF_{mod} = 46.2$  is close to the value  $FF_{ref} = 47.0$  %. The measured output power  $P_{MPP,mod} = 120$  mW for the module with an area  $A = 40$  cm<sup>2</sup> underlines the potential of the ISS technology.

## 4 CONCLUSIONS

We have examined different configurations of the in-situ series connection of thin film solar modules and compare their performance in respect to single cells prepared under similar conditions. The optimum configuration requires wire shifts directly before and after i-layer deposition. A flexible module with an area  $A = 40$  cm<sup>2</sup> and ten cells connected in series provides an output power  $P_{MPP,mod} = 120$  mW at an efficiency  $\eta_{mod} = 3.0$  % on a flexible PEN foil.

## ACKNOWLEDGEMENTS

Thanks to M. Sämann and C. Ehling for the developments of the single layers. We gratefully acknowledge financial support by the German Federal Ministry for the Environment, Nature Conservation and Nuclear Safety (BMU) under project no. 0325029.

## REFERENCES

- [1] J. J. Hanak, *Solar Energy* **23**, 145 (1979)
- [2] R. Merz, M. Schubert, J.H. Werner, in *Technical Digest 17th Int Photovolt. Spec. Conf.*, (Fukuoka, Japan, 2007), 971
- [3] Y. Gupta, H. Liers, S. Woods, S. Young, R. Deblasio, L. Mrig, in *Proc. 16th Photovolt. Spec. Conf.*, (IEEE, San Diego, 1982), p. 1092